

Provided for non-commercial research and education use.  
Not for reproduction, distribution or commercial use.



This article appeared in a journal published by Elsevier. The attached copy is furnished to the author for internal non-commercial research and education use, including for instruction at the authors institution and sharing with colleagues.

Other uses, including reproduction and distribution, or selling or licensing copies, or posting to personal, institutional or third party websites are prohibited.

In most cases authors are permitted to post their version of the article (e.g. in Word or Tex form) to their personal website or institutional repository. Authors requiring further information regarding Elsevier's archiving and manuscript policies are encouraged to visit:

<http://www.elsevier.com/authorsrights>



● *Original Contribution*

**DETERMINATION OF THE INTERFACIAL RHEOLOGICAL PROPERTIES OF  
 A POLY(DL-LACTIC ACID)-ENCAPSULATED CONTRAST AGENT USING  
 IN VITRO ATTENUATION AND SCATTERING**

SHIRSHENDU PAUL,\* DANIEL RUSSAKOW,\* TYLER RODGERS,\* KAUSIK SARKAR,\*<sup>†</sup> MICHAEL COCHRAN,<sup>‡</sup>  
 and MARGARET A. WHEATLEY<sup>‡</sup>

\*Department of Mechanical Engineering, University of Delaware, Newark, DE, USA; <sup>†</sup>Department of Mechanical and Aerospace Engineering, George Washington University Washington, DC, USA; and <sup>‡</sup>Department of Biomedical Engineering, Drexel University, Philadelphia, PA, USA

(Received 10 November 2012; revised 6 February 2013; in final form 11 February 2013)

**Abstract**—The stabilizing encapsulation of a microbubble-based ultrasound contrast agent (UCA) critically affects its acoustic properties. Polymers, which behave differently from materials commonly used (*i.e.*, lipids or proteins) for monolayer encapsulation, have the potential for better stability and improved control of encapsulation properties. Air-filled microbubbles coated with poly(DL-lactic acid) (PLA) are characterized here using *in vitro* acoustic experiments and several models of encapsulation. The interfacial rheological properties of the encapsulation are determined according to each model using attenuation of ultrasound through a suspension of microbubbles. Then the model predictions are compared with scattered non-linear (sub- and second harmonic) responses. For this microbubble population (average diameter, 1.9  $\mu\text{m}$ ), the peak in attenuation measurement indicates a weighted-average resonance frequency of 2.5–3 MHz, which, in contrast to other encapsulated microbubbles, is lower than the resonance frequency of a free bubble of similar size (diameter, 1.9  $\mu\text{m}$ ). This apparently contradictory result stems from the extremely low surface dilational elasticity (around 0.01–0.07 N/m) and the reduced surface tension of the poly(DL-lactic acid) encapsulation, as well as the polydispersity of the bubble population. All models considered here are shown to behave similarly even in the non-linear regime because of the low surface dilational elasticity value. Pressure-dependent scattering measurements at two different excitation frequencies (2.25 and 3 MHz) revealed strongly non-linear behavior with 25–30 dB and 5–20 dB enhancements in fundamental and second-harmonic responses, respectively, for a contrast agent concentration of 1.33  $\mu\text{g}/\text{mL}$  in the suspension. Sub-harmonic responses are registered above a relatively low generation threshold of 100–150 kPa, with up to 20 dB enhancement beyond that pressure. Numerical predictions from all models show good agreement with the experimentally measured fundamental response, but not with the experimental second-harmonic response. The characteristic features of sub-harmonic responses and the steady response beyond the threshold are matched well by model predictions. However, prediction of the threshold value depends on estimated properties and size distribution. The variation in size distribution from sample to sample leads to variation in estimates of encapsulation properties: the lowest estimated value for surface dilational viscosity better predicts the sub-harmonic threshold. (E-mail: [sarkar@gwu.edu](mailto:sarkar@gwu.edu)) © 2013 World Federation for Ultrasound in Medicine & Biology.

**Key Words:** Ultrasound, Contrast agents, Microbubbles, Poly(DL-lactic acid), Polymer shell, Sub-harmonic, Encapsulation, Resonance.

**INTRODUCTION**

Encapsulated microbubbles 1–10  $\mu\text{m}$  in diameter are used as contrast-enhancing agents for diagnostic ultrasound imaging. Encapsulating shells for ultrasound contrast agents (UCAs) are typically made of proteins (*e.g.*, Optison, GE Healthcare), lipids (*e.g.*, Definity, Lan-

thus Imaging; BR 14, SonoVue, Bracco Diagnostics; Sonazoid, GE Healthcare) and other common surfactants (Postema and Schmitz 2006). The shell stabilizes a microbubble against diffusion-driven dissolution, which would otherwise cause the microbubble to dissolve in a few milliseconds to seconds (Katiyar and Sarkar 2010; Katiyar et al. 2009; Sarkar et al. 2009). Recently, contrast agents with various polymeric shells have been developed that have the potential for enhanced stability (Eisenbrey et al. 2008; El-Sherif and Wheatley 2003; Pisani et al. 2006) and improved control of the encapsulation

Address correspondence to: Kausik Sarkar, George Washington University, 801 22nd Street NW, Academic Center, Washington, DC 20052, USA. E-mail: [sarkar@gwu.edu](mailto:sarkar@gwu.edu)

properties (Yang et al. 2009). Here we characterize and model linear and non-linear acoustic behaviors of poly(DL-lactic acid) (PLA)-encapsulated microbubbles.

Various polymeric microbubbles have been investigated for ultrasonic imaging (Forsberg et al. 2004; Grishenkov et al. 2009a, 2009b; Ketterling et al. 2007; Lavisse et al. 2005; Lu et al. 2009; Sciallero et al. 2012; Wheatley et al. 2007; Yang et al. 2009) and targeted drug delivery/therapeutics (Jie et al. 2008; Lu et al. 2009; Sirsi et al. 2009) (see the review by Xiong et al. [2011]). Specifically, PLA and poly(DL-lactic-co-glycolic acid) (PLGA), a block co-polymer with varying lactic/co-glycolic acid ratios, have been investigated as encapsulating materials for contrast microbubbles. An approximately 20 dB enhancement of acoustic response has been reported with PLGA (50:50 ratio of lactic acid to co-glycolic acid) contrast agents in both *in vitro* (El-Sherif and Wheatley 2003; Wheatley et al. 2006) and *in vivo* (Forsberg et al. 2004; Wheatley et al. 2006) dose-response studies. Forsberg and colleagues' study also investigated the role of varying ratios of lactic acid to glycolic acid in the PLGA *in vivo*. As lactic acid content was increased, the shell became more hydrophobic and increased in circulation time. These agents were conjugated with breast cancer-targeting ligands (Wheatley et al. 2007), making them a potential vehicle for cancer drug delivery. PLA-shelled contrast agents have also been loaded with the chemotherapeutic drug doxorubicin for ultrasound-mediated delivery (Eisenbrey et al. 2009, 2010a, 2010b). The maximum acoustic response achieved using drug-loaded contrast agents was an approximately 19 dB enhancement *in vitro* (at 5 MHz excitation and 690 kPa peak pressure) and an approximately 14 dB enhancement *in vivo* (with 5 MHz pulsed Doppler ultrasound) (Eisenbrey et al. 2010a). Size measurements on insonated doxorubicin-loaded contrast agents revealed a decrease in average size above the peak acoustic excitation pressure of 690 kPa, possibly as a result of bubble destruction through fragmentation or diffusive loss of gas (Eisenbrey et al. 2010b). Lavisse and co-workers (2005) have also independently studied PLA microparticles both *in vitro* and *in vivo* and reported an 18 dB enhancement in their *in vitro* dose-response studies conducted at 10 MHz and 275 kPa excitation.

A complete understanding of the key parameters contributing to stability, echogenicity and drug release requires reliable mathematical models. A number of models have been proposed to describe the dynamics of encapsulated microbubbles over the years (Chatterjee and Sarkar 2003; Church 1995; deJong et al. 1994; Doinikov and Dayton 2007; Hoff et al. 2000; Marmottant et al. 2005; Paul et al. 2010; Sarkar et al. 2005; Tsiglifis and Pelekasis 2008). To analyze and char-

acterize PLA-encapsulated microbubbles, we used four different interfacial rheological models (the first three developed in our lab): (i) Newtonian model; (ii) constant-elasticity model; (iii) strain-softening exponential elasticity model (Chatterjee and Sarkar 2003; Paul et al. 2010; Sarkar et al. 2005); and (iv) Marmottant model (Marmottant et al. 2005). These models have mostly been applied to predict the behavior of lipid-coated UCAs. Polymer-coated UCAs have been reported to behave differently, for example, to have lower elasticity than lipid- or protein-based contrast agents (Grishenkov et al. 2009a; Sciallero et al. 2012; Vos et al. 2007) or to have a resonance frequency lower than that of a similar-sized free bubble; typically, shell elasticity increases resonance frequency (Wheatley et al. 2006). Such distinct behaviors of polymeric microbubbles warrant further investigation. We have developed a hierarchical two-pronged approach to modeling, in which a model is applied to one set of experimental data to obtain model parameters, and then the model is validated against a second independent experiment (Chatterjee and Sarkar 2003; Paul et al. 2010; Sarkar et al. 2005). Model improvement/modification is initiated as warranted by the process of validation.

Here the same process of mechanical characterization using interfacial rheological models of encapsulation is applied to PLA microbubbles. Model parameters are determined using attenuation, and then the model predictions are compared against scattering, specifically non-linear second- and sub-harmonic scattering. Non-linear scattering from these PLA microbubbles has not been measured before. Resonance frequency, threshold for sub-harmonic generation and the latter's critical dependence on bubble size are investigated. In the next section is a description of the materials and methods followed by a brief overview of the mathematical modeling and simulations. In the third section, we present and discuss the experimental and modeling results, and in the final section, we summarize the results.

## METHODS

### *Microbubble preparation*

Poly(lactic acid) UCAs were fabricated using a double-emulsion technique (El-Sherif and Wheatley 2003). Five hundred milligrams of PLA (100 DL MW = 83 kDa; Lakeshore Biomaterials, Birmingham, AL, USA) was dissolved in 10 mL of methylene chloride (Fisher Scientific, Waltham, MA, USA) along with 50 mg of camphor (Sigma-Aldrich, St. Louis, MO, USA). When the polymer was completely dissolved, 1 mL of ammonium carbonate solution (4% w/v; J.T. Baker, Phillipsburg, NJ, USA) was added to the polymer solution, which was immediately sonicated on ice for 30 s (10

pulses of 3 s each separated by 1 s) with 110 W applied power (CL4 tapped horn probe with 0.5-in. tip [Misonix, Farmingdale, NY, USA]). The resulting water-in-oil emulsion was immediately added to 50 mL of a cold 5% (w/v) poly(vinyl) alcohol solution (Polysciences, Warrington, PA, USA) and homogenized for 5 min at 9500 rpm with a sawtooth homogenizer probe (Brinkmann Instruments, Westbury, NY, USA). Immediately after homogenization, 100 mL of 2% (v/v) isopropyl alcohol (Fisher Scientific) was added to the emulsion, which was stirred for 1 h to allow the methylene chloride to evaporate. The particles were then collected by centrifugation at 2500 g for 5 min and washed three times with hexane (Fisher Scientific). After any residual hexane was allowed to evaporate, the particles were washed in water, then flash-frozen and lyophilized for 48 h with a Benchtop freeze dryer (VirTis, Gardiner, NY, USA). The water and ammonium carbonate from the core of the particles and the camphor from the polymer shell were allowed to sublimate during lyophilization to create a porous polymer shell encapsulating a void that is filled with air when the microbubbles are returned to atmospheric pressure. Contrast agent in the form of a dry powder was refrigerated and stored until ready for use.

#### Size distribution measurement

The size distribution was measured by dynamic light scattering using a Zetasizer Nano ZS (Malvern Instruments, Worcestershire, UK). One milligram of dry contrast agent was suspended in 1 mL phosphate-buffered saline by vortexing for 10 s then transferred into a disposable cuvette and allowed to equilibrate for 3 min before measurements were made.

#### Experimental setup to measure attenuation

The experimental setup for attenuation measurement used a pulse-echo system at room temperature (Fig. 1a) (Chatterjee *et al.* 2005a, 2005b; Paul *et al.* 2012). Attenuation from a suspension of contrast agent (constantly stirred) was measured using three different unfocused broadband transducers (Olympus NDT, Waltham, MA, USA) with central frequencies 2.25 MHz (V306-SU), 3.5 MHz (V382-SU) and 5 MHz (V309-SU) operating in transmit/receive mode. The -6 dB bandwidth ranges of the transducers were 1.178–3.32, 2.5–4.99 and 3.13–6.19 MHz, respectively. A pulser/receiver (Model 5800; Panametrics-NDT, Waltham, MA, USA) was used to excite the transducers at a pulse repetition frequency of 100 Hz; it generated a broadband pulse of duration of 440 ns. The pulse generated at the face of the transducer traveled a total distance of 12 cm through the contrast agent suspension (from the transducer face to the container wall and back; container is made of 1.17-cm-thick polycarbonate sheet) before being

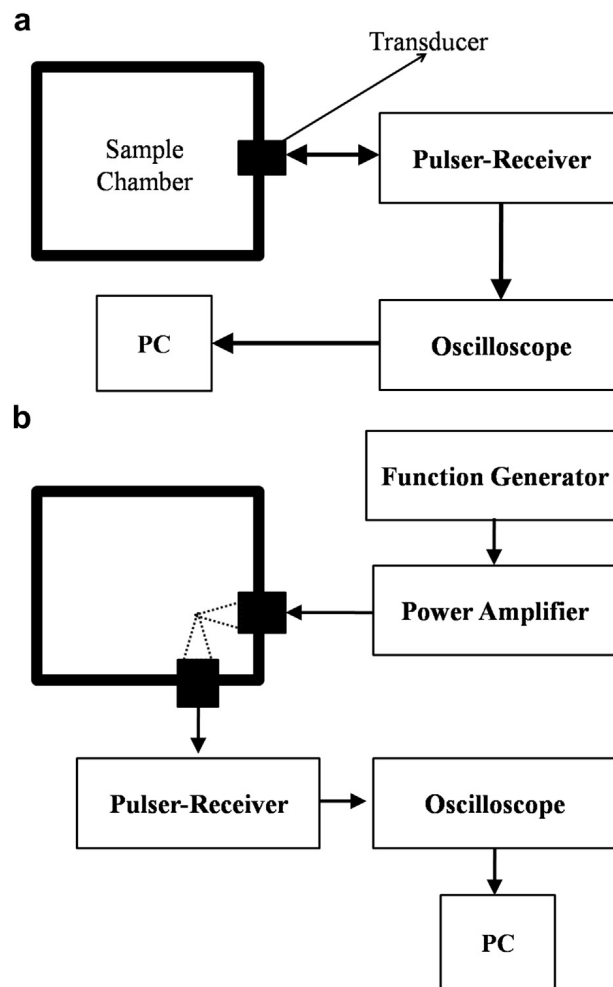


Fig. 1. Schematic of the experimental setup for *in vitro* measurement of (a) attenuation and (b) scattering.

received and fed to the digital oscilloscope (Model TDS 2012; Tektronix, Beaverton, OR, USA) to observe the signal in real time. Signals were acquired from the oscilloscope *via* a GPIB IEEE 488 cable and a GPIB card and saved on a desktop computer using LabView (Version 6.0.3; National Instruments, Austin, TX, USA). Twenty voltage–time radiofrequency traces were acquired in an averaging mode (64 sequences are used for averaging) and saved. The data were then analyzed using Matlab (Mathworks, Natick, MA, USA) to calculate the attenuation coefficient for the contrast agent suspension. The excitation amplitude, 200 kPa peak negative pressure, is low enough so that the frequency-dependent broadband attenuation does not depend on the acoustic pressure (Chatterjee *et al.* 2005b); that is, lowering the excitation did not affect it.

#### Experimental setup to measure scattering

The scattering setup (Fig. 1b) used was similar to that used by previous researchers (Nahire *et al.* 2012; Paul *et al.* 2012; Sarkar *et al.* 2005; Shi and Forsberg

2000). It employed two spherically focused transducers, each having an individual diameter of 1.6 cm and focal length of 3.05 cm. We confocally positioned the transmitting and receiving transducers at right angles by placing them through circular holes drilled through the adjacent walls of a rectangular chamber. This configuration ensures similarity of scattered signals to backscattered echoes (Shi and Forsberg 2000) along with high spatial resolution (Sarkar et al. 2005). One hundred fifty milliliters of contrast agent suspension was required for complete immersion of both transducers. Two different transmitting transducers (Olympus NDT) were employed with center frequencies of 3.62 MHz (V382 1.2-in. point target focus (PTF)) and 2.35 MHz (V306 1.2-in. PTF) and respective -6 dB bandwidths of 83.84% and 80.68%. Another focused transducer with a center frequency of 5.54 MHz (V309 1.2-in. PTF) and -6 dB bandwidth of 85.06% was used to receive the scattered signal. An arbitrary/function generator (Model AFG 3251, Tektronix) was used to generate a 32-cycle sinusoidal pulse of desired frequency (2.25 and 3.5 MHz for this study) at a pulse repetition frequency of 100 Hz. This signal was then amplified using a 55 dB power amplifier (Model A-300, ENI, Rochester, NY, USA) and fed to the transmitting transducer. A 0.4-mm needle hydrophone (PZT-Z44-0400, Onda, CA, USA) was used to calibrate transducers. The contrast agent at the focal volume of the transducer scattered back this signal, which was received by the receiving transducer using a pulser/receiver (Model 5800, Panametrics-NDT) in receiving mode with a 20 dB gain. The amplified signals were then fed to the oscilloscope to view them in real time. Voltage-time radiofrequency signals were saved onto the desktop with the same method used for attenuation experiments. For data analysis of the scattered signals, 50 acquisitions in averaging mode were saved on the computer.

#### Experimental procedure and data reduction

Contrast agent in the form of a dry powder was refrigerated and stored until ready for use. The dry powder was reconstituted in phosphate-buffered saline (PBS) to make a stock solution with a concentration of 1 mg powder/mL PBS (equivalent to a bubble concentration of  $30 \times 10^6$  bubbles/mL). This stock solution was subsequently used to achieve desired dilutions during acoustic experiments. Attenuation measurements were acquired for a range of contrast agent concentrations between 0.5 and 3.5  $\mu\text{g/mL}$ . All scattering measurements were conducted at a concentration of 1.33  $\mu\text{g/mL}$ . The stock solution was pipetted into the container with PBS (previously left to equilibrate for 5–10 min to equilibrate with atmospheric oxygen concentration and to get rid of any air bubbles created). A 200  $\mu\text{L}$  aliquot of stock

sample was carefully added by automatic pipet and allowed to mix for around 10 s using a magnetic stirrer to ensure a homogeneous suspension before application of ultrasound. The stirring was continued through the entire course of the experiment to maintain homogeneity. Readings taken of the sample without contrast agents revealed no interference from entrained bubbles. The total volume of gas added with the agent was less than 100  $\mu\text{L}$  in a total volume of 150 mL. Each attenuation and scattering experiment was repeated five times; that is, five data sets were collected from five new suspensions prepared from the stock solution freshly taken into the experimental setups.

For attenuation, signals were obtained with and without UCAs. A Matlab code was used to convert each of the voltage-time responses acquired to frequency domain using fast Fourier transform (FFT), and then 20 acquisitions were averaged. The attenuation coefficient was calculated using the expression

$$\alpha(\omega) = 20 \log_{10} \left( \frac{\overline{V}_{ref}(\omega)}{\overline{V}_{sig}(\omega)} \right) / d, \quad (1)$$

where  $\overline{V}_{ref}(\omega)$  is the averaged response in the frequency domain without any contrast agent in the medium;  $\overline{V}_{sig}(\omega)$  is the averaged response in the frequency domain with microbubbles suspended in the medium; and  $d$ , the total path traveled by the pulse before it is received by the transducer.

For the time-dependent attenuation study, a total of 200 voltage-time acquisitions were obtained for study over a 20 min period. Acoustic excitation was started as soon as the PLA-encapsulated contrast agents were pipetted into the PBS solution and stirred for 10 s to attain homogeneity. Attenuation was averaged over each successive 30 s interval. We computed the time-dependent total attenuation normalized by its initial value using

$$NA(t) = \frac{A(t)}{A(0)}; A = 10 \log_{10} \left( \frac{\sum_{\omega} V_{ref}^2(\omega)}{\sum_{\omega} V_{sig}^2(\omega)} \right) / d. \quad (2)$$

Note that such a (summed-over-frequency) measure can be used even at higher excitation amplitudes, unlike the frequency-dependent attenuation (eqn [1]), which would be corrupted by non-linear energy transfer across frequency spectrum (Chatterjee et al. 2005a).

For scattering, a similar technique was used to get the average response in the frequency domain (50 voltage-time acquisitions were used). The scattered response was converted into a decibel scale by taking the reference voltage to be unity. Responses at frequencies of interest were then appropriately extracted from

the resultant data set to find the fundamental, second- and sub-harmonic scattered responses.

*Mathematical modeling*

The dynamics of an encapsulated microbubble are governed by a Rayleigh–Plesset (RP)-type equation. Many models have been proposed to describe the effects of the encapsulating shell of contrast microbubbles. Recently, we showed that all models, including those that represent the shell as having a finite thickness and consisting of materials with bulk material properties, can be expressed in a single interfacial framework. The framework contributes two additional interfacial stress terms to the RP equation: effective surface tension,  $\gamma(R)$  and encapsulation dilational viscosity,  $\kappa^s(R)$  (Katiyar and Sarkar 2011):

$$\rho \left( R\ddot{R} + \frac{3}{2}\dot{R}^2 \right) = P_{G_0} \left( \frac{R_0}{R} \right)^{3k} \left( 1 - \frac{3k\dot{R}}{c} \right) - \frac{2}{R} \gamma(R) - \frac{4\dot{R}}{R^2} \kappa^s(R) - 4\mu \frac{\dot{R}}{R} - p_0 + p_A(t). \quad (3)$$

$R$  is the time-dependent bubble radius;  $\dot{R}$  and  $\ddot{R}$  are the first- and second-order time derivatives of the bubble radius respectively;  $c$  is the velocity of sound in the surrounding liquid;  $\rho$  is the liquid density;  $\mu$  is the liquid viscosity;  $R_0$  is the initial bubble radius;  $P_{G_0}$  is the initial inside gas pressure;  $p_0$  is the ambient pressure; and  $p_A(t)$  is the excitation pressure. Gas diffusion is neglected. The inside gas pressure obeys a polytropic law with index  $k$ . We use four different models for encapsulation:

**1. Newtonian model (NM) (Chatterjee and Sarkar 2003)**

$$\gamma(R) = \gamma(\text{constant}) \text{ and } \kappa^s(R) = \kappa^s(\text{constant}). \quad (4)$$

**2. Constant-elasticity viscoelastic model (CEM) (Chatterjee et al. 2005a)**

$$\gamma(R) = \begin{cases} \gamma_0 + E^s \beta & \text{for } \gamma_0 + E^s \beta > 0 \\ 0 & \text{for } \gamma_0 + E^s \beta \leq 0 \end{cases} \text{ and } \kappa^s(R) = \kappa^s(\text{constant}), \quad (6)$$

Here,  $\gamma_0$  is the constant interfacial tension;  $E^s$  is the constant dilational elasticity; and  $\beta = (\Delta \text{Area} / \text{Area}_{\text{equilibrium}}) = (R^2 / R_E^2 - 1)$ . The equilibrium radius  $R_E$  is given by  $R_E = R_0(1 - \gamma_0 / E^s)^{-1/2}$ . This ensures a balance between inside and outside pressure at the initial radius. At the equilibrium radius, the bubble encapsulation has no elastic stresses. Resonance frequency  $f_0$  is

$$f_0 = \frac{1}{2\pi R_0} \sqrt{\frac{1}{\rho} \left( 3kp_0 - \frac{4\gamma_0}{R_0} + \frac{4E^s}{R_0} \right)}. \quad (7)$$

**3. Viscoelastic model with exponentially varying elasticity (EEM) (Paul et al. 2010)**

$$\gamma(R) = \begin{cases} \gamma_0 + E^s \beta & \text{for } \gamma_0 + E^s \beta > 0 \\ 0 & \text{for } \gamma_0 + E^s \beta \leq 0 \end{cases} \text{ and } \kappa^s(R) = \kappa^s(\text{constant}), \quad (8)$$

Here,  $\gamma_0$  is the constant interfacial tension;  $E^s = E_0^s \beta \exp(-\alpha^s \beta)$ ; and  $\beta = R^2 / R_E^2 - 1$ . Enforcing the balance of pressure at the initial radius, we have an expression for equilibrium:

$$R_E = R_0 \left[ 1 + \left( \frac{1 - \sqrt{1 + 4\gamma_0 \alpha^s / E_0^s}}{2\alpha} \right) \right]^{-1/2}.$$

The expression for resonance frequency  $f_0$  is

$$f_0 = \frac{1}{2\pi R_0} \sqrt{\frac{1}{\rho} \left( 3kp_0 + \frac{2E_0^s}{R_0} \left( \frac{\sqrt{1 + 4\gamma_0 \alpha^s / E_0^s}}{\alpha^s} \right) \left( 1 + 2\alpha^s - \sqrt{1 + 4\gamma_0 \alpha^s / E_0^s} \right) \right)}. \quad (9)$$

The resonance frequency ( $f_0$ ) of a bubble can be obtained from the linearized dynamics and is

**4. Marmottant model (MM) (Marmottant et al. 2005)**

$$\gamma(R) = \begin{cases} 0 & \text{for } R \leq R_{\text{buckling}} \\ \chi \left( \frac{R^2}{R_{\text{buckling}}^2} - 1 \right) & \text{for } R_{\text{buckling}} \leq R \leq R_{\text{rupture}} \\ \gamma_w & \text{for } R \geq R_{\text{rupture}} \end{cases} \text{ and } \kappa^s(R) = \kappa^s(\text{constant}), \quad (10)$$

Here,  $\chi$  (same as  $E^s$  in eqn 6) is the elastic modulus of the shell;  $R_{buckling} = R_0[1 + \gamma(R_0)/\chi]^{-1/2}$ ; and  $R_{rupture} = R_{buckling}[1 + \gamma_\omega/\chi]^{1/2}$ . Above  $R_{rupture}$ , the bubble is assumed to have a pure air-water interface, and below  $R_{buckling}$ , it is in a buckled state where the effective interfacial tension is zero. The expression for resonance frequency  $f_0$  is

$$f_0 = \frac{1}{2\pi R_0} \sqrt{\frac{1}{\rho} \left( 3kp_0 + \frac{2\gamma(R_0)}{R_0} (3k-1) + \frac{4\chi}{R_0} \right)}. \quad (11)$$

### Estimation of model parameters

We developed a method for using the attenuation data measured to determine the parameters of the encapsulation models (Chatterjee and Sarkar 2003; Paul et al. 2010; Sarkar et al. 2005). The low-amplitude excitation used to measure attenuation ensures that the attenuation data are collected in the linear regime of bubble dynamics. The linearized form of the modified RP equation was used to determine resonance frequency (according to eqn [5], [7], [9] or [11]) and the damping for each model. For our simulations, we used  $\rho = 1000 \text{ kg/m}^3$ ,  $\mu = 0.001 \text{ kg/m}\cdot\text{s}$ ,  $c = 1485 \text{ m/s}$  and  $p_0 = 101325 \text{ Pa}$ . We assumed isothermal behavior for the air inside,  $k = 1.0$ , which is appropriate for the size of microbubbles studied here (Brenner et al. 2002; Hilgenfeldt et al. 1998; Prosperetti 1977b). With knowledge of the damping and size distribution, we derived an expression for attenuation through a suspension of contrast microbubbles. An error function between the measured attenuation  $\alpha^{meas}(\omega_i)$  and the modeled attenuation  $\alpha(\omega_i)$  was formulated:

$$Er(\gamma, \kappa^s, \dots) = \sum_i [\alpha(\omega_i) - \alpha^{meas}(\omega_i)]^2 \quad (12)$$

Model parameters were obtained through minimization of this error function using Matlab. (Refer to previous publications by Sarkar and co-workers [Paul et al. 2010; Sarkar et al. 2005] for a detailed discussion of the parameter estimation technique.)

### Prediction of scattering

With the estimated expressions for surface tension,  $\gamma(R)$  and dilational surface viscosity,  $\kappa^S(R)$ , corresponding to a particular encapsulation model, the modified RP equation was solved for varying acoustic pressure amplitudes ( $P_A$ ) using Matlab with initial conditions  $R(t=0) = R_0$  and  $\dot{R}(t=0) = 0$ . The scattered pressure,  $P_S(t)$ , and the scattering cross section were calculated from the radial dynamics using the expressions (Brennen 1995; Paul et al. 2010).

$$P_S(r, t) = \rho \frac{R}{r} (2\dot{R}^2 + R\ddot{R}) \quad \text{and} \quad \sigma_s(r, t) = \frac{4\pi \langle r^2 P_S(r, t)^2 \rangle}{P_A}. \quad (13)$$

With fast Fourier transform (FFT), the computed scattered power was converted into the frequency domain, and the total scattered power spectrum from the bubble suspension was calculated, integrating the contribution from bubbles of all radii from  $R_{min}$  to  $R_{max}$ :

$$S_s(\omega) = \int_{R_{min}}^{R_{max}} \sigma_s(R; \omega) n(R) dR. \quad (14)$$

Here,  $n(R)$  is the number of microbubbles per unit volume per unit radius. The peak values corresponding to different frequencies (*i.e.*, fundamental, second- and sub-harmonic) were then extracted from the power spectrum to match experimental results. The predicted fundamental response for both excitation frequencies was matched to the experimentally measured response for the lowest acoustic pressure to account for the scattering volume and plotted and compared with experimental results. This same matching constant was also used to rescale the predicted second- and sub-harmonic responses and plotted for comparison with experiments.

## RESULTS AND DISCUSSION

### Size distribution

Figure 2 and Table 1 outline the size distribution measurements for three different samples acquired from the same stock solution using dynamic light scattering equipment as described previously. Number-averaged diameters (see Table 1) are similar for all three measurements, except for the slightly lower value for sample 3. However, note that the distribution for sample 3 is

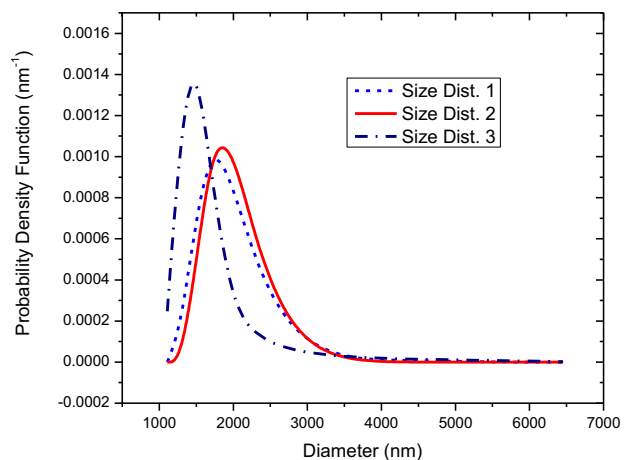


Fig. 2. Three independent measurements of the size distribution of poly(DL-lactic acid)-encapsulated contrast microbubbles obtained using dynamic light scattering.

Table 1. Size distributions, z-averaged\* diameters and number-averaged diameters for three separate measurements of poly(DL-lactic acid)-encapsulated microbubbles obtained using dynamic light scattering

	Size distribution 1 (%)	Size distribution 2 (%)	Size distribution 3 (%)
Diameter (nm)			
1106	0.0	0	4
1281	3.0	0	21.1
1484	14.9	9.8	33.2
1718	27.4	27.6	21.3
1990	25.1	30.5	7.7
2305	16.1	19.4	4.3
2689	8.3	9.2	2.7
3091	3.4	3	1.8
3580	0.9	0.5	1.3
4145	0.5	0	1.0
4801	0.4	0	0.8
5560	0	0	0.6
6439	0	0	0.2
Average diameter			
Number-averaged	1999 nm	2030 nm	1726 nm
z-Averaged	3486 nm	3377 nm	3151 nm

\* Defined by Malvern as “the intensity weighted mean of the hydrodynamic size of the ensemble collection of particles.”

markedly different from those for the other two samples, with a tighter size distribution, lower peak diameter and smaller number of bubbles above 1500 nm. Instead of using an average distribution, we used all three size distributions in our analysis and investigated the effects of size distribution variation on estimation of parameters and prediction of scattering. We see below that the difference in size distributions leads to different predictions of sub-harmonic response.

#### Attenuation and estimation of interfacial rheological properties

Attenuation measurements were obtained for five different concentrations of contrast agent using all three transducers. Frequency-dependent attenuation coefficients plotted for each measurement were generated using the data reduction technique explained earlier. The value of the attenuation coefficient corresponding to the center frequency of each transducer was then extracted. The average value for each set of five experiments, along with the corresponding standard deviation, was then plotted in Figure 3a. Note that for the range of concentrations studied here, attenuation increased linearly for all three transducers used, indicating minimal effects of multiple scattering for the dilute concentrations considered. Figure 3b illustrates the frequency-dependent attenuation coefficient obtained for the highest concentration for three different transducers. Attenuation coefficients obtained with different transducers are similar in the region of their overlapping bandwidth frequencies. The peak of the attenuation curve occurs

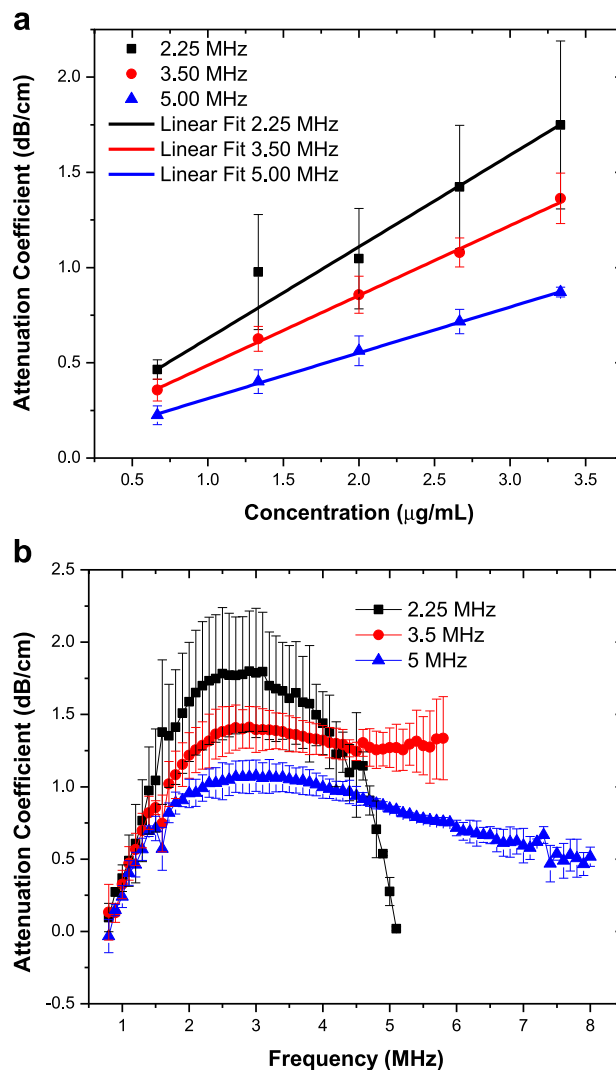


Fig. 3. (a) Attenuation coefficient at the central frequencies of the three transducers (2.25, 3.5 and 5 MHz) as a function of microbubble concentration (averaged over five different acquisitions). (b) Frequency-dependent attenuation coefficient measured with three different transducers (with central frequencies 2.25, 3.5 and 5 MHz) averaged over five different acquisitions.

around 2.5–3 MHz, indicating a weighted-average resonance frequency for the polydispersed sample within this range.

Using the method described earlier, we calculated the unknown parameters pertaining to each model (see Table 2) using the three different size distributions. Note that for the MM, we assumed that the contrast agent is initially in a buckled state with zero surface tension; this would render it initially stable in the absence of acoustic excitation. The frequency-dependent attenuation curves obtained through modeling (using each bubble size distribution) match very well with experiment. We show the match only for the NM (Fig. 4); others are very similar and are not shown for brevity. However,

Table 2. Values for parameters of poly(DL-lactic acid)-encapsulated microbubbles obtained using three different models and three different size distributions

Encapsulation model	Estimated parameter		
	Size distribution 1	Size distribution 2	Size distribution 3
Newtonian model	$\gamma = 0.08 \text{ N/m}$ $\kappa^s = 7.5 \times 10^{-9} \text{ N}\cdot\text{s/m}$	$\gamma = 0.06 \text{ N/m}$ $\kappa^s = 8.5 \times 10^{-9} \text{ N}\cdot\text{s/m}$	$\gamma = 0.03 \text{ N/m}$ $\kappa^s = 2.0 \times 10^{-9} \text{ N}\cdot\text{s/m}$
Viscoelastic constant-elasticity model	$\gamma_0 = 0.02 \text{ N/m}$ $E^s = 0.07 \text{ N/m}$ $\kappa^s = 7.5 \times 10^{-9} \text{ N}\cdot\text{s/m}$	$\gamma_0 = 0.01 \text{ N/m}$ $E^s = 0.05 \text{ N/m}$ $\kappa^s = 8.5 \times 10^{-9} \text{ N}\cdot\text{s/m}$	$\gamma_0 = 0.01 \text{ N/m}$ $E^s = 0.02 \text{ N/m}$ $\kappa^s = 2.1 \times 10^{-9} \text{ N}\cdot\text{s/m}$
Viscoelastic exponential elasticity model	$\gamma_0 = 0.02 \text{ N/m}$ $E_0^s = 0.07 \text{ N/m}$ $\alpha = 1.5$ $\kappa^s = 7.5 \times 10^{-9} \text{ N}\cdot\text{s/m}$	$\gamma_0 = 0.01 \text{ N/m}$ $E_0^s = 0.05 \text{ N/m}$ $\alpha = 1.5$ $\kappa^s = 8.5 \times 10^{-9} \text{ N}\cdot\text{s/m}$	$\gamma_0 = 0.01 \text{ N/m}$ $E_0^s = 0.02 \text{ N/m}$ $\alpha = 1.5$ $\kappa^s = 2.1 \times 10^{-9} \text{ N}\cdot\text{s/m}$
Marmottant model	$\gamma_0 = 0.00 \text{ N/m}$ $\chi = 0.08 \text{ N/m}$ $\kappa^s = 7.5 \times 10^{-9} \text{ N}\cdot\text{s/m}$	$\gamma_0 = 0.00 \text{ N/m}$ $\chi = 0.06 \text{ N/m}$ $\kappa^s = 8.5 \times 10^{-9} \text{ N}\cdot\text{s/m}$	$\gamma_0 = 0.00 \text{ N/m}$ $\chi = 0.04 \text{ N/m}$ $\kappa^s = 2.0 \times 10^{-9} \text{ N}\cdot\text{s/m}$

note that unlike in our previous experience (Paul et al. 2010), using average size and total number did not work very well in estimating the parameters; depending on the initial guesses for the parameters at the start of minimization, often the error minimization procedure did not converge, and when it converged, it gave rise to unphysical values for the material parameters. The inability to use an average diameter for parameter estimation indicates the importance of the polydispersity of the bubble size distribution and the limitation of the estimation process adopted here. One has to be careful in adopting such a process and interpreting the results.

The estimated parameters for the three different size distributions are similar except for the slightly smaller dilational viscosity for size distribution 3. (Note also the slightly smaller surface tension value for this distribution, but only for the NM.) The smaller dilational viscosity for distribution 3 can be explained by noting that damping of

a bubble increases as radius decreases (Katiyar and Sarkar 2011, 2012). Size distribution 3 has the largest fraction of smaller bubbles. Therefore, the same attenuation data gave rise to the smallest damping for this distribution. Note that the interfacial elasticity values predicted for PLA-coated microbubbles (0.02–0.07 N/m) are an order of magnitude smaller than the values reported previously for phospholipid-coated bubbles (~0.5 N/m) (Paul et al. 2010; Sarkar et al. 2005; van der Meer et al. 2007). However, the interfacial viscosity values ( $2 \times 10^{-9}$  to  $8.5 \times 10^{-9} \text{ kg/s}$ ) are similar to those reported in the literature for other bubbles. Using size distribution 3 predicts the lowest values for surface dilational viscosity and, therefore, correspondingly the lowest damping, which critically affects the sub-harmonic response from microbubbles as is discussed later. Note that unlike Sonazoid, here we obtained a reasonable value for surface tension,  $\gamma$ , even for the NM. For the other models, the surface tension value ( $\gamma_0$ ) was lower than the air–water interface value ( $\gamma_w = 0.07 \text{ N/m}$ ). The low surface tension, along with an extremely low elasticity value, contributes to the low average resonance frequency seen for these microbubbles.

*Resonance frequency*

Figure 3b illustrates that the measured attenuation increases with increasing frequency, reaching a peak in the range 2.5–3 MHz — indicating the incidence of average resonance frequency there — and decreases thereafter. Because the response of a bubble is considerably higher at its resonance frequency, the peak in attenuation occurs there. However, note that the reasoning holds strictly for a monodisperse bubble population. The frequency for the peak response agrees well with the previously reported value of 2.28 MHz (El-Sherif 2003). As noted before, the resonance frequency of the PLA bubble was reported to be lower than that of a same-sized free bubble, in contrast to other contrast

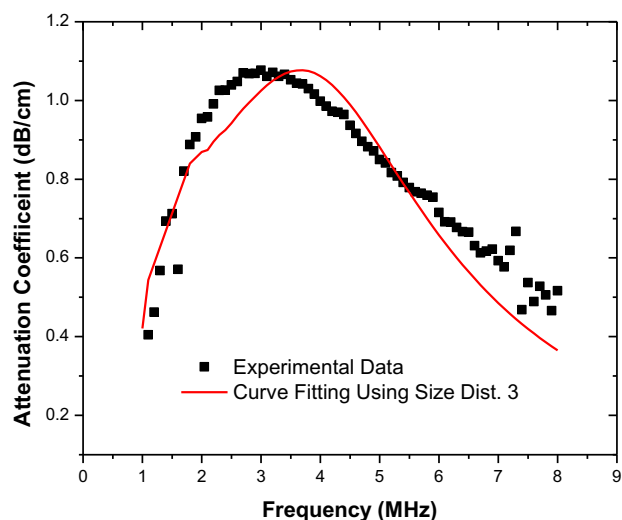


Fig. 4. Experimentally measured attenuation and prediction by the Newtonian model obtained during parameter estimation using sample 3 size distribution.

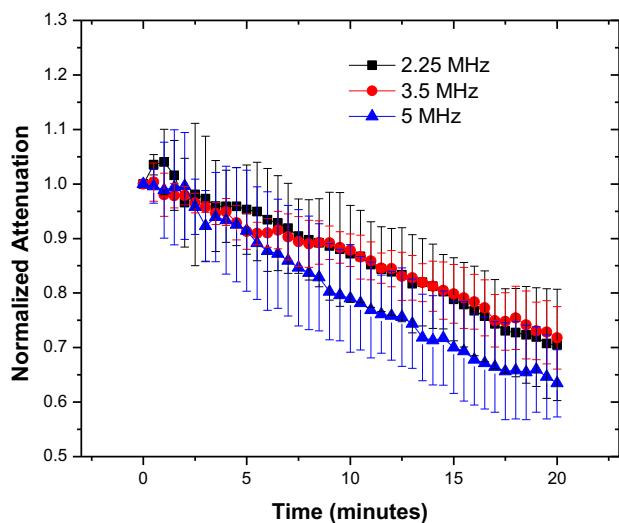


Fig. 5. Plot of normalized total attenuation coefficient versus time. The data were averaged over five different acquisitions each collected continuously and averaged over consecutive 30 second intervals.

microbubbles for which the elasticity of the encapsulation increases stiffness, giving rise to a higher resonance frequency (van der Meer *et al.* 2007). The resonance frequency of a free bubble is often estimated using the well-known Minneart formula:

$$f_{\text{Minneart}}(\text{MHz}) \approx \frac{3.26}{R_0(\mu\text{m})} \quad (15)$$

However, note that this formula is more appropriate for bubbles that are millimeters or larger in size; it includes only the term for gas compressibility—the first term inside the bracket in eqn (5)—and neglects the contribution of surface tension. The surface tension term increases for bubbles of micrometer size and is of the same order as the compressibility term. For a free air bubble in water with an average diameter of  $1.9 \mu\text{m}$ , resonance frequency computed with the Minneart formula (3.43 MHz) increases significantly (5.01 MHz) when corrected for surface tension effects. Therefore, the decrease in resonance frequency with encapsulation is even greater (Wheatley *et al.* 2006), when one would expect the encapsulation to contribute to the stiffness of the damped mass-spring system and increase its resonance frequency. As we mentioned above, this paradox was noted before (Wheatley *et al.* 2006), and several hypotheses have been proposed to explain it, for example, presence of gas-filled cells with an average diameter less than that of the entire capsule, or a highly porous capsule in which tiny chambers make a greater contribution to the actual dynamics or a disproportionate contribution from bubbles of different sizes to the overall dynamics. Note, however, that a smaller effective radius would lead to an even higher resonance frequency.

We argue that the result stems from several effects: the reduced surface tension,  $\gamma_0$ , the extremely small dilational surface elasticity and the polydispersity of the size distribution, which makes the average diameter irrelevant in determining average parameters. This explains the difficulty in estimating parameters using average diameter described above. The attenuation curve with its maximum peak position results from attenuation of bubbles of different sizes from the entire size distribution, which includes a small number of larger bubbles different in size from the average of the size distribution. These bubbles have their peak attenuation at a frequency lower than that corresponding to the average size. Using only the average radius, therefore, inevitably leads to a larger resonance frequency, as it neglects the effects of these larger bubbles. Note also that non-linearity can decrease resonance frequency (Doinikov *et al.* 2009; Overvelde *et al.* 2010); for lipid-shelled microbubbles, it tends to decrease with increasing acoustic excitation pressure. We see in subsequent sections that the non-linearity of PLA-encapsulated bubbles sets in at much lower excitation pressures (around 100–150 kPa).

#### *Time-dependent attenuation*

Sustained acoustic excitation changes the state of the encapsulation, which in turn affects bubble stability and lifetime (Eisenbrey *et al.* 2008). To investigate bubble lifetime under acoustic excitation, attenuation was measured as a function of time and plotted in Figure 5, which shows a steady decrease with time, as was also observed previously (Casciaro *et al.* 2007; Chatterjee *et al.* 2005a; Krasovitski *et al.* 2004). Contrast agents containing gases other than air cause a transient increase in attenuation initially before an eventual decrease. The increase in attenuation is caused by the transient growth of bubble volume, because initially the air diffuses into the bubbles much faster than the low-solubility gases diffuse outward (Shi and Forsberg 2000). Air-filled PLA agents do not show such a transient increase. We observed that over the 20-min period, attenuation dropped by 30%–40%. Also note that in previous time response backscatter studies with PLA (El-Sherif and Wheatley 2003) and PLGA (50:50) (Wheatley *et al.* 2006) contrast microbubbles, a 15% loss in enhancement was reported over the same time period.

#### *Scattering and comparison with model prediction*

*Fundamental and second-harmonic responses.* Scattered responses from PLA-encapsulated contrast agents were acquired at varying acoustic pressure amplitudes at two different excitation frequencies, 3.5 and 2.25 MHz. Averages and standard deviations of five

independent acquisitions at each pressure amplitude were then calculated with the aforementioned data analysis technique. Fundamental (at excitation frequency), second-harmonic (at twice the excitation frequency) and sub-harmonic (at half the excitation frequency) responses for both transducers are shown in Figure 6a–c.

The fundamental response shows a 25–30 dB enhancement in the entire range of excitations for both frequencies. Similar enhancement was reported in previous *in vitro* scattering experiments with PLA microbubbles: an approximately 17 dB enhancement at 5 MHz and 690 kPa excitation pressure (estimated from the dose–response curve for 1.33  $\mu\text{g}/\text{mL}$ ) (Eisenbrey et al. 2010a). For a PLGA (50:50) microbubble, enhancement was 10 dB at 2.25 MHz and 20 dB at 5 MHz (Wheatley et al. 2006). For the second harmonic, the enhancement was 10–35 dB (2.25 MHz) and 5–25 dB (3.5 MHz). These results reflect the echogenicity of PLA agents, specifically their efficacy in harmonic contrast imaging, where the second-harmonic response is imaged.

Both fundamental (Fig. 6a) and second-harmonic (Fig. 6b) responses (plotted on a log–log scale) for each excitation frequency increase approximately linearly with increasing acoustic pressures. They deviate from linearity at higher pressure; in particular, the second-harmonic response curve flattens beyond 320 kPa, possibly because of bubble destruction. The slopes for the curves were found to be 0.92 at 3.5 MHz and 1.15 at 2.25 MHz for the fundamental response and about 1.5 at both frequencies for the second-harmonic response. Small-amplitude perturbation analysis predicts them to be 1 (fundamental) and 2 (second harmonic). However, the experimentally measured slope of the second harmonic has been shown to deviate from its theoretical value of 2 (Shi and Forsberg 2000).

We also simulated the scattered response from the microbubbles using several models. Note that for each model, we obtained three different predictions, using three different sets of parameter values obtained with the three different size distributions given in Table 1 and Figure 2. The scattered responses were computed using the corresponding size distributions. For both excitation frequencies, the predicted fundamental responses from all three models (Fig. 7a, b) are in good agreement with experimental data for all three bubble distributions (size distributions 1–3). The experimental curve deviates from model predictions at higher pressures. The deviation occurs approximately around the same pressure (320 kPa) where the linearity of the experimental result breaks down possibly because of bubble destruction (Chatterjee et al. 2005a). Destruction is not accounted for in any of the models, which might explain the difference between model predictions and experimental observations.

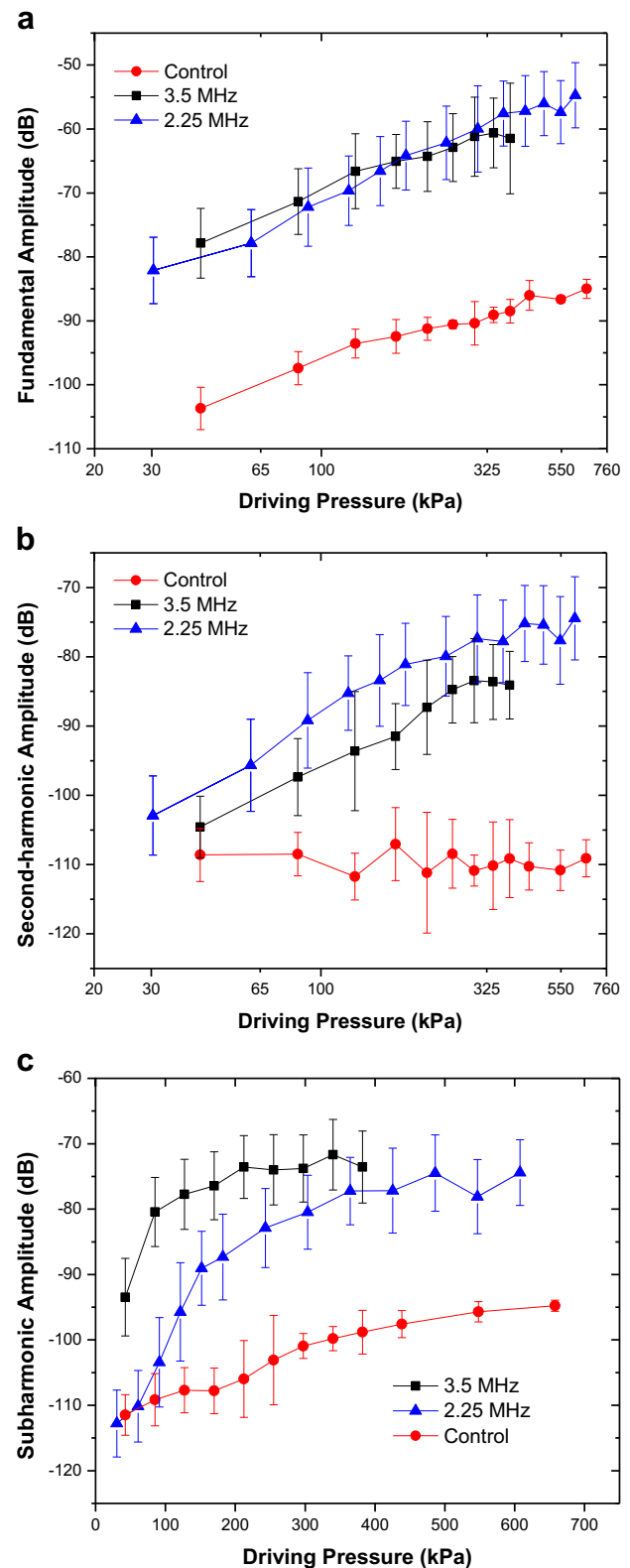


Fig. 6. Experimentally measured scattered responses of PLA-encapsulated microbubbles at two different excitation frequencies (2.25 and 3.5 MHz): (a) fundamental; (b) second harmonic; (c) sub-harmonic. Control represents data obtained without any bubbles introduced.

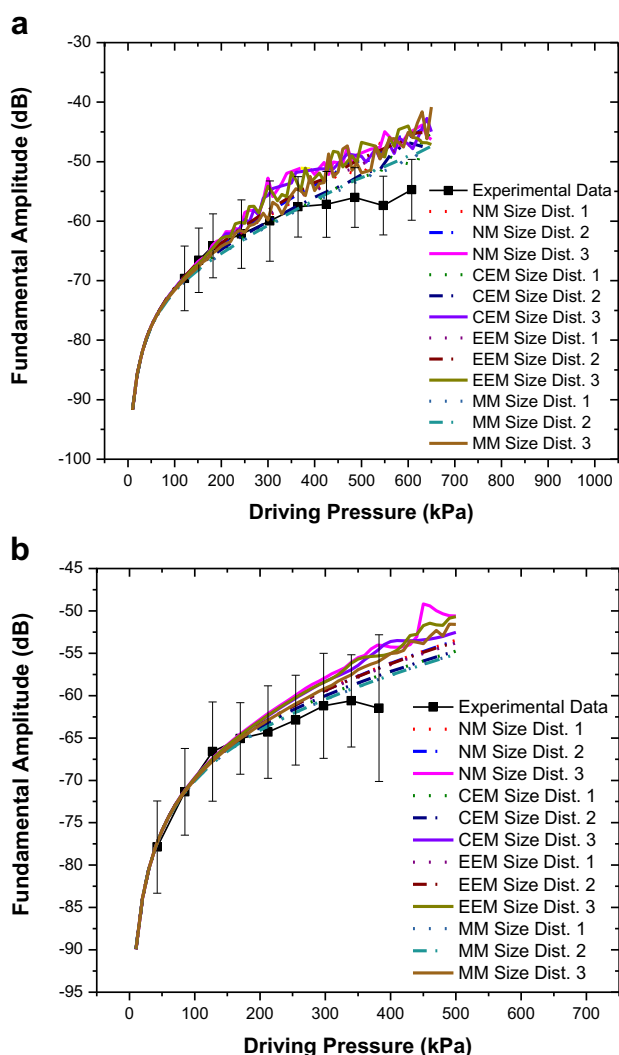


Fig. 7. Comparison of experimentally measured and predicted scattered fundamental responses of PLA-encapsulated microbubbles for different models using three different size distributions at (a) 2.25-MHz excitation and (b) 3.5-MHz excitation.

Second-harmonic responses predicted by the different models have a slope of 2, as they should, in contrast to the experiments as noted before (Fig. 8a, b). They do not match very well even for lower acoustic pressures. However, the predictions from all three models and three size distributions are similar. Note that the second-harmonic frequencies studied here are within the receiving bandwidth of the transducer used. The discrepancy in the model prediction points to inadequacies of the modeling effort. Also, as mentioned before, the bubble destruction that might affect the non-linear response was not accounted for in the models.

*Sub-harmonic response.* The scattered sub-harmonic responses from PLA microbubbles (Fig. 6c) at both frequencies are typical: initially no sub-harmonic before a threshold pressure value and, at

threshold, a rapid rise followed by saturation (Sarkar *et al.* 2005; Shi and Forsberg 2000). The excitation threshold at an excitation frequency of 2.25 MHz is 125 kPa, slightly higher than the 100 kPa at 3.5 MHz. Classical bubble dynamics theory predicts a minimum threshold for sub-harmonic generation to be at twice the resonance frequency (Eller and Flynn 1968; Neppiras 1969; Prosperetti 1977a). Observations for two different encapsulated microbubbles—Optison (Shankar *et al.* 1999) and Definity (Kimmel *et al.* 2007)—were reported to be in line with this theory. The frequency for the minimum sub-harmonic threshold for PLA agents is therefore expected to be between 5 and 6 MHz. Note, however, that we have recently shown that the minimum threshold shifts toward resonance, away from twice its value, for encapsulated microbubbles because of large damping (Katiyar and Sarkar 2012). We also showed that the threshold is rather flat in the region between resonance and twice its value. We note that the threshold at 3.5 MHz is only slightly lower than that at 2.25 MHz.

All models considered here predict very low acoustic responses until the threshold is reached (Fig. 9a, b). Hence, model predictions are shown only when above  $-120$  dB (above the noise level,  $-115$  dB, of the experimental measurement). Unlike the fundamental response, the simulated sub-harmonic response does not have an unqualified match for all bubble distributions. Note that the post-threshold response level is matched well for both frequencies. However, the predicted threshold value varies. For both frequencies, size distributions 1 and 2 exhibit much higher threshold values in comparison to experimental data (see Table 3). Size distribution 3, which has a larger fraction of smaller bubbles (Fig. 2), matches very well (solid curves) the threshold for 2.25-MHz excitation and is closer to the experimentally measured threshold for 3.5 MHz.

#### Model validation and predictive capability

In our previous modeling exercise, we emphasized the need for independent model validation (Chatterjee and Sarkar 2003; Paul *et al.* 2010; Sarkar *et al.* 2005). We determined the model parameters through linear attenuation data, as is done here, and then validated the model by investigating its ability to predict sub-harmonic responses obtained at higher excitations. In fact, our modeling exercise led to results that dictated model improvements from the NM to the CEM to the EEM. For Alunex, Optison and Sonazoid (Chatterjee and Sarkar 2003), the NM resulted in an unrealistically large surface tension value and, hence, was deemed unsuitable for modeling encapsulated microbubbles. As a result, we introduced surface dilatational elasticity (Sarkar *et al.* 2005). However, here we find a very low value of surface dilatational elasticity for PLA

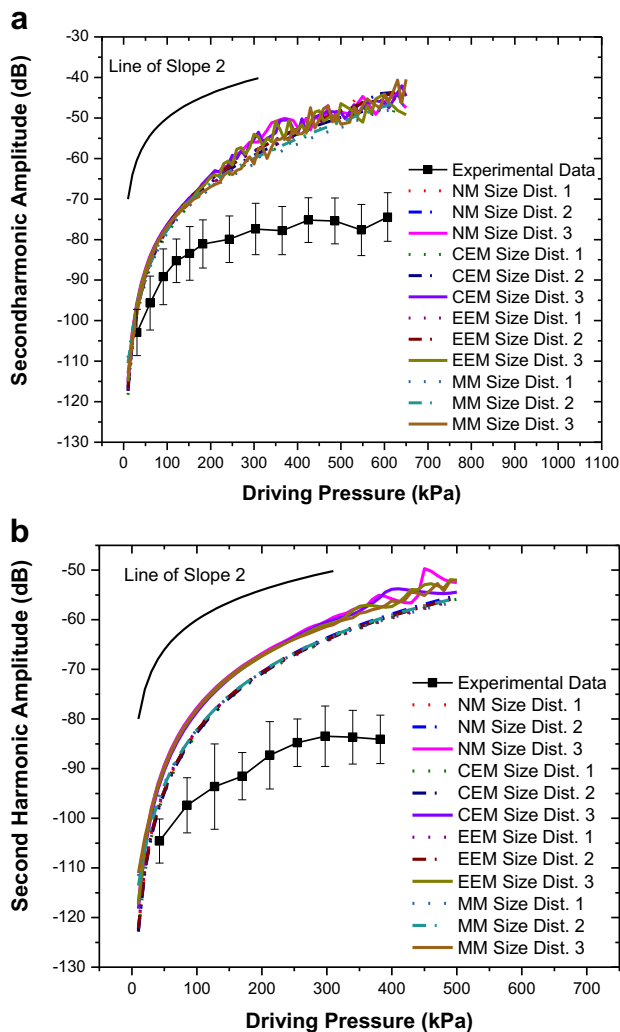


Fig. 8. Comparison of experimentally measured and predicted scattered second-harmonic responses of PLA-encapsulated microbubbles for different models at (a) 2.25-MHz excitation and (b) 3.5-MHz excitation. A line with a slope of 2 is also shown for comparison. NM = Newtonian model, CEM = constant-elasticity model, EEM = exponential elasticity model, MM = Marmottant model.

encapsulation. Even the NM predicts low surface tension values; for size distribution 3, it predicted a value lower than that for the air–water interface. As mentioned above, only for size distribution 3 did we get a prediction that matched experimentally measured thresholds. For this distribution all models predicted similar values: the CEM and MM predicted slightly higher values than the NM and EEM, the latter two predicting the same value. The NM therefore remains an effective model to describe PLA bubbles. We use it below to examine further certain features of PLA-encapsulated microbubbles.

We note that all models perform poorly in predicting second-harmonic responses, and clearly more research is needed to resolve this discrepancy. However, for predict-

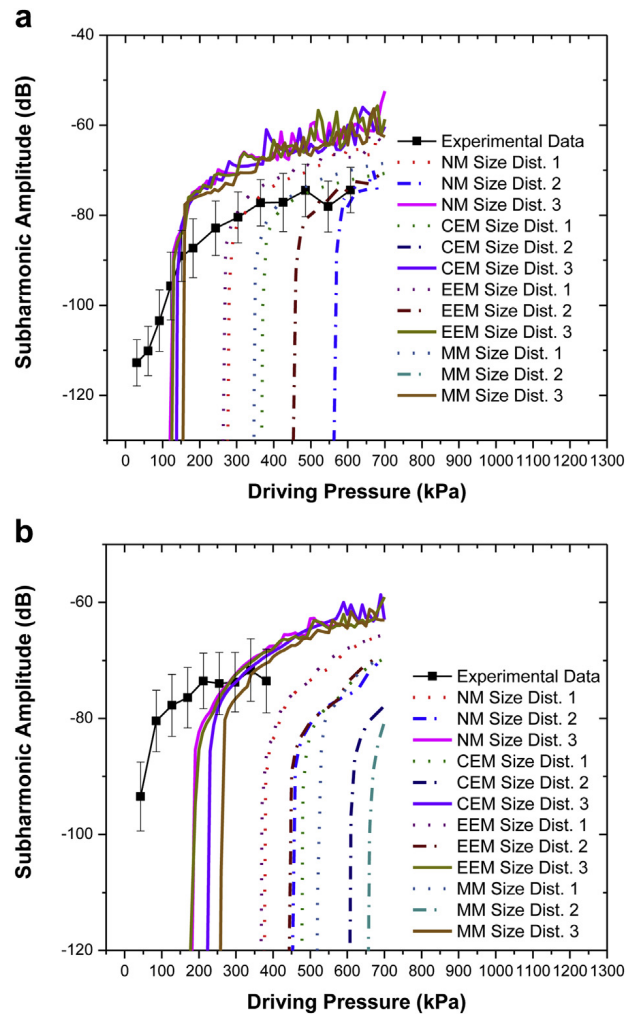


Fig. 9. Comparison of experimentally measured and predicted scattered sub-harmonic responses of PLA-encapsulated microbubbles for different models at (a) 2.25-MHz excitation and (b) 3.5-MHz excitation. The curves for CEM and MM, size distribution 2, at 2.25 MHz have thresholds too high to be seen here. NM = Newtonian model, CEM = constant-elasticity model, EEM = exponential elasticity model, MM = Marmottant model.

ing sub-harmonic responses, size distribution 3 fares the best (see Table 3 for sub-harmonic threshold), indicating that the behavior of any model describing the dynamics of encapsulated microbubbles is critically dependent on bubble size distribution. (As mentioned above, such extreme sensitivity in size distribution, where in fact the different size distributions were obtained from the same batch, also insinuates the limitations of the parameter estimation technique used.) Specifically, the sub-harmonic threshold depends on the ratio of excitation frequency to natural frequency, and natural frequency is determined by bubble size (Katiyar and Sarkar 2011). More bubbles with lower sub-harmonic threshold values would lower the overall threshold value as well. Also, as

Table 3. Threshold pressure for sub-harmonic generation obtained experimentally and using three different models for all three size distributions studied

	Threshold pressure (kPa)	
	2.25 MHz	3.5 MHz
Experiment	125	100
Newtonian model		
Size distribution 1	280	380
Size distribution 2	570	460
Size distribution 3	<b>130</b>	<b>190</b>
Viscoelastic constant-elasticity model		
Size distribution 1	370	480
Size distribution 2	1500	610
Size distribution 3	<b>140</b>	<b>230</b>
Viscoelastic exponential elasticity model		
Size distribution 1	270	370
Size distribution 2	460	450
Size distribution 3	<b>130</b>	<b>190</b>
Marmottant model		
Size distribution 1	350	520
Size distribution 2	830	660
Size distribution 3	<b>160</b>	<b>250</b>

Values in bold indicate the lowest predicted subharmonic generation thresholds corresponding to each encapsulation models.

we already noted, the variation in size distribution from sample to sample affected corresponding parameters for the three samples; sample 3 had the lowest surface dilational viscosity value: one-third to one-fourth those of the other two samples. Decreased damping lowers the sub-harmonic generation threshold (Katiyar and Sarkar 2011, 2012). To further investigate the effects of material parameters and size distribution on the predicted sub-harmonic response, we used the material properties (low dilational viscosity value,  $\kappa^s = 2.0 \times 10^{-9} \text{ N}\cdot\text{s/m}$ ) determined using size distribution 3, but computed sub-harmonic response with all distributions including distributions 1 and 2. The results illustrated in Figure 10 (a, b) indicate that the lower dilational viscosity predicts sub-harmonic responses closer to the experimentally measured value, even with the other two size distributions. We therefore conclude that the lower dilational viscosity (albeit determined with the size distribution corresponding to sample 3) is the critical factor. This underscores the fact that accurate estimation of the average material parameters of encapsulation critically depends on the ability to measure the size distribution, and inter-sample variation has to be taken into account (Commander and Prosperetti 1989).

### CONCLUSIONS

In this article, we characterized PLA-coated air-containing microbubbles through *in vitro* scattering and attenuation experiments. Four different models of microbubble encapsulation—Newtonian, constant-elasticity,

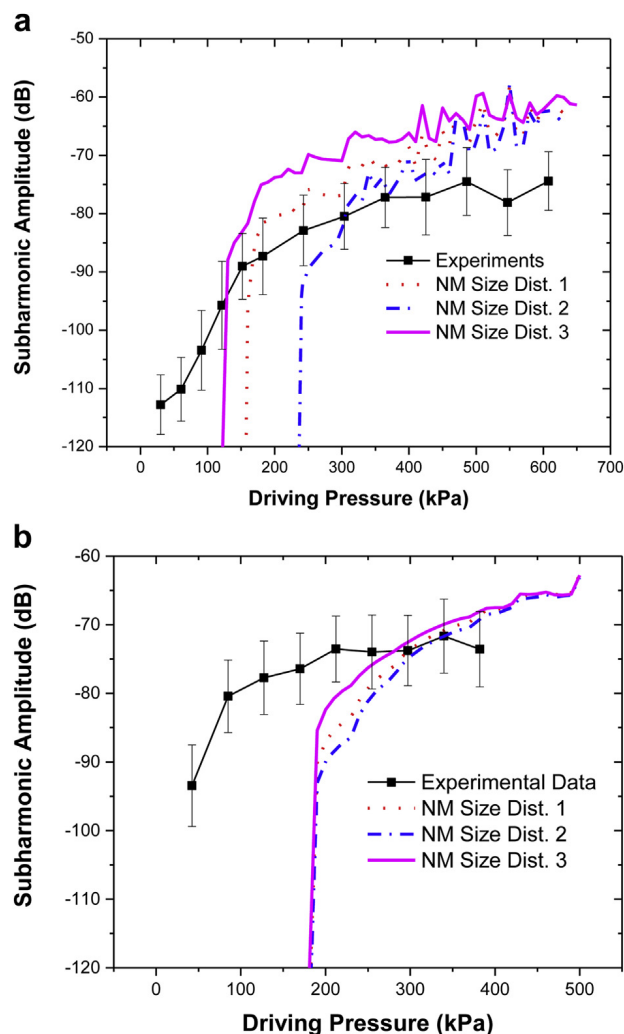


Fig. 10. Comparison of experimentally measured and predicted scattered sub-harmonic responses of PLA-encapsulated microbubbles for the Newtonian model (NM) with different size distributions and sample 3 parameter values at (a) 2.25-MHz excitation and (b) 3.5-MHz excitation.

exponential elasticity and Marmottant—were used to determine the interfacial rheological properties of the microbubble. Unlike our previous investigation of Sonazoid and Optison, we found low values for interfacial tension and surface dilational elasticity, which explains the similar results (and similar parameter values) for all models. However, sample-to-sample size distribution variations for the same batch of contrast agents gives rise to variation in the parameters determined using them.

The peak in the attenuation spectrum indicates a weighted-average resonance at around 2.5–3 MHz, in agreement with previous measurements. As noted before, this value for average resonance frequency is smaller than that of a free bubble of the same size (1.9  $\mu\text{m}$  in diameter). We discussed in detail the limitations of the Minneart formula for microbubbles, showing that the reduced

resonance frequency stems from the reduced surface tension, extremely low surface elasticity and polydispersity; normally, the surface elasticity of an encapsulation results in enhanced stiffness of the system, thereby increasing resonance frequency. The low interfacial elasticity value distinguishes PLA-encapsulated bubbles from other lipid- and protein-coated bubbles.

Poly(DL-lactic acid)-encapsulated microbubbles have both second- and sub-harmonic scattered responses as a result of non-linear oscillations. All models predict similar dynamics and match the fundamental scattered response very well, but fail to predict the second-harmonic response, clearly indicating the need for further research. Experimentally measured second-harmonic responses have a slope of 1.5 in contrast to the theoretical value of 2. The sub-harmonic response exhibits the characteristic features: it appears only above a threshold excitation level (100–150 kPa) and then sharply rises with increasing excitation strength. The models predict the characteristic features of a sub-harmonic response and the post-threshold response amplitude. The size variation from sample to sample gives rise to variation in parameters, in particular for surface dilational viscosity. The lower value for surface dilational viscosity obtained using one of the measured size distributions results in better prediction of the experimentally measured sub-harmonic threshold value.

This experimental and modeling study of PLA-coated contrast microbubbles using two independent acoustic experiments—linear attenuation for model determination and non-linear scattering for validation—revealed several unique features of PLA-coated microbubbles, such as extremely low encapsulation elasticity values and relatively low sub-harmonic threshold values and explains the low resonance frequency experimentally observed here as well as before. Our study also indicates that contrast microbubbles are polydisperse complex systems and underscores the importance of careful analysis of experiments performed on them.

*Acknowledgments*—K.S. acknowledges financial support from National Science Foundation Grants CBET-0651912, CBET-1033256, DMR-1239105 and CBET-1205322 and National Institutes of Health Grant P20 RR016472.

## REFERENCES

- Brennen CE. Cavitation and bubble dynamics. New York: Oxford University Press; 1995.
- Brenner MP, Hilgenfeldt S, Lohse D. Single-bubble sonoluminescence. *Rev Mod Phys* 2002;74:425–484.
- Casciaro S, Errico RP, Conversano F, Demitri C, Distante A. Experimental investigations of nonlinearities and destruction mechanisms of an experimental phospholipid-based ultrasound contrast agent. *Invest Radiol* 2007;42:95–104.
- Chatterjee D, Jain P, Sarkar K. Ultrasound-mediated destruction of contrast microbubbles used for medical imaging and drug delivery. *Phys Fluids* 2005a;17:100603.
- Chatterjee D, Sarkar KA. Newtonian rheological model for the interface of microbubble contrast agents. *Ultrasound Med Biol* 2003;29:1749–1757.
- Chatterjee D, Sarkar K, Jain P, Schreppler NE. On the suitability of broadband attenuation measurement for characterizing contrast microbubbles. *Ultrasound Med Biol* 2005b;31:781–786.
- Church CC. The effects of an elastic solid-surface layer on the radial pulsations of gas-bubbles. *J Acoust Soc Am* 1995;97:1510–1521.
- Commander KW, Prosperetti A. Linear pressure waves in bubbly liquids: Comparison between theory and experiments. *Journal of the Acoustical Society of America* 1989;85:732–746.
- DeJong N, Cornet R, Lancee CT. Higher harmonics of vibrating gas-filled microspheres: 1. Simulations. *Ultrasonics* 1994;32:447–53.
- Doinikov AA, Dayton PA. Maxwell rheological model for lipid-shelled ultrasound microbubble contrast agents. *J Acoust Soc Am* 2007;121:3331–3340.
- Doinikov AA, Haac JF, Dayton PA. Resonance frequencies of lipid-shelled microbubbles in the regime of nonlinear oscillations. *Ultrasonics* 2009;49:263–268.
- Eisenbrey JR, Burstein OM, Kambhampati R, Forsberg F, Liu JB, Wheatley MA. Development and optimization of a doxorubicin loaded poly(lactic acid) contrast agent for ultrasound directed drug delivery. *J Control Release* 2010a;143:38–44.
- Eisenbrey JR, Burstein OM, Wheatley MA. Effect of molecular weight and end capping on poly(lactic-co-glycolic acid) ultrasound contrast agents. *Polym Eng Sci* 2008;48:1785–1792.
- Eisenbrey JR, Huang P, Hsu J, Wheatley MA. Ultrasound triggered cell death in vitro with doxorubicin loaded poly lactic-acid contrast agents. *Ultrasonics* 2009;49:628–633.
- Eisenbrey JR, Soulen MC, Wheatley MA. Delivery of encapsulated doxorubicin by ultrasound-mediated size reduction of drug-loaded polymer contrast agents. *IEEE Trans Bio-Med Eng* 2010b;57:24–28.
- El-Sherif D. Development of novel PLGA contrast agents for use as ultrasound targeted drug delivery vehicles. PhD Thesis, Drexel University, Philadelphia 2003.
- El-Sherif DM, Wheatley MA. Development of a novel method for synthesis of a polymeric ultrasound contrast agent. *J Biomed Mater Res A* 2003;66:347–355.
- Eller A, Flynn HG. Generation of subharmonics of order one-half by bubbles in a sound field. *J Acoust Soc Am* 1968;44:368–369.
- Forsberg F, Lathia JD, Merton DA, Liu JB, Le NT, Goldberg BB, Wheatley MA. Effect of shell type on the in vivo backscatter from polymer-encapsulated microbubbles. *Ultrasound Med Biol* 2004;30:1281–1287.
- Grishenkov D, Pecorari C, Brismar TB, Paradossi G. Characterization of acoustic properties of PVA-shelled ultrasound contrast agents: Linear properties (Part I). *Ultrasound Med Biol* 2009a;35:1127–1138.
- Grishenkov D, Pecorari C, Brismar TB, Paradossi G. Characterization of acoustic properties of PVA-shelled ultrasound contrast agents: Ultrasound-induced fracture (Part II). *Ultrasound Med Biol* 2009b;35:1139–1147.
- Hilgenfeldt S, Lohse D, Zomack M. Response of bubbles to diagnostic ultrasound: A unifying theoretical approach. *Eur Phys J B* 1998;4:247–255.
- Hoff L, Sontum PC, Hovem JM. Oscillations of polymeric microbubbles: Effect of the encapsulating shell. *J Acoust Soc Am* 2000;107:2272–2280.
- Jie P, Zhenqing H, Peijuan Z, Yange W, Qian W, Qiqing Z. Optimization of production of PLA microbubble ultrasound contrast agents for hydroxycamptothecin delivery. *BioMedical Engineering and Informatics* 2008;400–406.
- Katiyar A, Sarkar K. Stability analysis of an encapsulated microbubble against gas diffusion. *J Colloid Interface Sci* 2010;343:42–47.
- Katiyar A, Sarkar K. Excitation threshold for subharmonic generation from contrast microbubbles. *J Acoust Soc Am* 2011;130:3137–3147.
- Katiyar A, Sarkar K. Effects of encapsulation damping on the excitation threshold for subharmonic generation from contrast microbubbles. *J Acoust Soc Am* 2012;132:3576–3585.
- Katiyar A, Sarkar K, Jain P. Effects of encapsulation elasticity on the stability of an encapsulated microbubble. *J Colloid Interface Sci* 2009;336:519–525.

- Ketterling JA, Mamou J, Allen JS, Aristizabal O, Williamson RG, Turnbull DH. Excitation of polymer-shelled contrast agents with high-frequency ultrasound. *J Acoust Soc Am* 2007;121:E148–E153.
- Kimmel E, Krasovitski B, Hoogi A, Razansky D, Adam D. Subharmonic response of encapsulated microbubbles: Conditions for existence and amplification. *Ultrasound Med Biol* 2007;33:1767–1776.
- Krasovitski B, Kimmel E, Sapunar M, Adam D. Ultrasound attenuation by encapsulated microbubbles: Time and pressure effects. *Ultrasound Med Biol* 2004;30:793–802.
- Lavisse S, Paci A, Rouffiac V, Adotevi C, Opolon P, Peronneau P, Bourget P, Roche A, Perricaudet M, Fattal E, Lassau N. In vitro echogenicity characterization of poly[lactide-coglycolide] (PLGA) microparticles and preliminary in vivo ultrasound enhancement study for ultrasound contrast agent application. *Invest Radiol* 2005;40:536–544.
- Lu JM, Wang XW, Marin-Muller C, Wang H, Lin PH, Yao QZ, Chen CY. Current advances in research and clinical applications of PLGA-based nanotechnology. *Expert Rev Mol Diagn* 2009;9:325–341.
- Marmottant P, van der Meer S, Emmer M, Versluis M, de Jong N, Hilgenfeldt S, Lohse D. A model for large amplitude oscillations of coated bubbles accounting for buckling and rupture. *J Acoust Soc Am* 2005;118:3499–3505.
- Nahire R, Paul S, Scott MD, Singh RK, Muhonen WW, Shabb J, Gange KN, Srivastava DK, Sarkar K, Mallik S. Ultrasound enhanced matrix metalloproteinase-9 triggered release of contents from echogenic liposomes. *Mol Pharm* 2012;9:2554–2564.
- Neppiras EA. Subharmonic and other low-frequency emission from gas bubbles in sound-irradiated liquids. *J Acoust Soc Am* 1969;46:587–601.
- Overvelde M, Garbin V, Sijl J, Dollet B, de Jong N, Lohse D, Versluis M. Nonlinear Shell Behavior of Phospholipid-Coated Microbubbles. *Ultrasound Med Biol* 2010;36:2080–2092.
- Paul S, Katiyar A, Sarkar K, Chatterjee D, Shi WT, Forsberg F. Material characterization of the encapsulation of an ultrasound contrast microbubble and its subharmonic response: Strain-softening interfacial elasticity model. *J Acoust Soc Am* 2010;127:3846–3857.
- Paul S, Russakow D, Nahire R, Nandy T, Ambre AH, Katti K, Mallik S, Sarkar K. In vitro measurement of attenuation and nonlinear scattering from echogenic liposomes. *Ultrasonics* 2012;52:962–969.
- Pisani E, Tsapis N, Paris J, Nicolas V, Cattell L, Fattal E. Polymeric nano/microcapsules of liquid perfluorocarbons for ultrasonic imaging: Physical characterization. *Langmuir* 2006;22:4397–4402.
- Postema M, Schmitz G. Bubble dynamics involved in ultrasonic imaging. *Expert Rev Mol Diagn* 2006;6:493–502.
- Prosperetti A. Application of subharmonic threshold to measurement of damping of oscillating gas-bubbles. *J Acoust Soc Am* 1977a;61:11–16.
- Prosperetti A. Thermal effects and damping mechanisms in the forced radial oscillations of gas bubbles in liquids. *J Acoust Soc Am* 1977b;61:17–27.
- Sarkar K, Katiyar A, Jain P. Growth and dissolution of an encapsulated contrast microbubble. *Ultrasound Med Biol* 2009;35:1385–1396.
- Sarkar K, Shi WT, Chatterjee D, Forsberg F. Characterization of ultrasound contrast microbubbles using in vitro experiments and viscous and viscoelastic interface models for encapsulation. *J Acoust Soc Am* 2005;118:539–550.
- Sciallero C, Paradossi G, Trucco A. A preliminary in vitro assessment of polymer-shelled microbubbles in contrast-enhanced ultrasound imaging. *Ultrasonics* 2012;52:456–464.
- Shankar PM, Krishna PD, Newhouse VL. Subharmonic backscattering from ultrasound contrast agents. *J Acoust Soc Am* 1999;106:2104–2110.
- Shi WT, Forsberg F. Ultrasonic characterization of the nonlinear properties of contrast microbubbles. *Ultrasound Med Biol* 2000;26:93–104.
- Sirsi SR, Schray RC, Wheatley MA, Lutz GJ. Formulation of polylactide-co-glycolic acid nanospheres for encapsulation and sustained release of poly(ethylene imine)–poly(ethylene glycol) copolymers complexed to oligonucleotides. *J Nanobiotechnol* 2009;7:1.
- Tsiglilifis K, Pelekasis NA. Nonlinear radial oscillations of encapsulated microbubbles subject to ultrasound: The effect of membrane constitutive law. *J Acoust Soc Am* 2008;123:4059–4070.
- Van der Meer SM, Dollet B, Voormolen MM, Chin CT, Bouakaz A, de Jong N, Versluis M, Lohse D. Microbubble spectroscopy of ultrasound contrast agents. *J Acoust Soc Am* 2007;121:648–656.
- Vos HJ, Guidi F, Boni E, Tortoli P. Method for microbubble characterization using primary radiation force. *IEEE Trans Ultrason Ferroelectr Freq Control* 2007;54:1333–1345.
- Wheatley MA, Forsberg F, Oum K, Ro R, El-Sherif D. Comparison of in vitro and in vivo acoustic response of a novel 50:50 PLGA contrast agent. *Ultrasonics* 2006;44:360–367.
- Wheatley MA, Lathia JD, Oum KL. Polymeric ultrasound contrast agents targeted to integrins: Importance of process methods and surface density of ligands. *Biomacromolecules* 2007;8:516–522.
- Xiong XY, Zhao FL, Shi MR, Yang H, Liu YY. Polymeric microbubbles for ultrasonic molecular imaging and targeted therapeutics. *J Biomater Sci Polym E* 2011;22:417–428.
- Yang F, Li Y, Chen Z, Gu N. The preparation and application of microbubble contrast agent combining ultrasound imaging and magnetic resonance imaging. *Chin Sci Bull* 2009;54:2934–2939.